

Journal of Biomedical Optics

SPIDigitalLibrary.org/jbo

Polarized light imaging in biomedicine: emerging Mueller matrix methodologies for bulk tissue assessment

Sanaz Alali
Alex Vitkin



SPIE

Polarized light imaging in biomedicine: emerging Mueller matrix methodologies for bulk tissue assessment

Sanaz Alali^a and Alex Vitkin^{a,b,*}

^aUniversity of Toronto, Division of Biophysics and Bioimaging, Ontario Cancer Institute/University Health Network and Department of Medical Biophysics, 101 College Street, Toronto, Ontario M5G 1L7, Canada

^bUniversity of Toronto, Department of Radiation Oncology, 610 University Avenue, Toronto, Ontario M5G 2M9, Canada

Abstract. Polarized light point measurements and wide-field imaging have been studied for many years in an effort to develop accurate and information-rich tissue diagnostic methods. However, the extensive depolarization of polarized light in thick biological tissues has limited the success of these investigations. Recently, advances in technology and conceptual understanding have led to a significant resurgence of research activity in the promising field of bulk tissue polarimetry. In particular, with the advent of improved measurement, analysis, and interpretation methods, including Mueller matrix decomposition, new diagnostic avenues, such as quantification of microstructural anisotropy in bulk tissues, have been enabled. Further, novel technologies have improved the speed and the accuracy of polarimetric instruments for *ex vivo* and *in vivo* diagnostics. In this paper, we review some of the recent progress in tissue polarimetry, provide illustrative application examples, and offer an outlook to the future of polarized light imaging in bulk biological tissues. © 2015 Society of Photo-Optical Instrumentation Engineers (SPIE)

[DOI: [10.1117/1.JBO.20.6.061104](https://doi.org/10.1117/1.JBO.20.6.061104)]

Keywords: polarized light imaging; Mueller matrix; bulk tissue microstructure.

Paper 140808SSR received Dec. 5, 2014; accepted for publication Jan. 29, 2015; published online Mar. 20, 2015.

1 Polarized Light in Biomedicine

Optical imaging modalities in biomedicine offer insight into tissue structure (down to cellular or even subcellular level) and function (metabolic and compositional information, microvascular blood flow), often by providing bulk tissue properties, such as absorption or scattering, which can be used to detect and differentiate tissue pathology. To obtain this wealth of useful biophysical insights, an optical imaging modality measures a specific change in the amplitude, phase, wavelength, or polarization of light reflected, transmitted, absorbed, or remitted from tissue (often as a function of space and/or time). One of these optical characterization methods is polarimetry, which is the science of studying polarized light interaction with materials to infer information about their structure and composition. In addition to biological tissues, polarimetric methods have been extensively used in industry for characterizing thin films, semiconductor chips, chemical content of food/drugs, and for aerosol sensing applications.¹⁻³

One particularly important tissue property, well suited for polarimetric measurements, is its microstructural anisotropy (asymmetry). Many diseases are associated with microstructural alterations, such as changes in collagen content and organization, muscular hypertrophy/atrophy, or perhaps cellular orientations. These structural abnormalities can present changes in linear birefringence that can be detected by polarized light. Using polarized light to image collagen fibrils in thin tissue microscopy goes back to the 1960s.^{4,5} Today, many other

uses of polarized light in biomedicine have emerged, most often as an add-on option (in combination with other optical imaging modalities), such as polarization-sensitive hyperspectral imaging, polarization-sensitive optical coherence tomography (PS-OCT), polarization-sensitive fluorescence microscopy, and polarization-sensitive multiphoton microscopy.⁶⁻¹⁰ For example, a well-established clinical application of polarized light is imaging the anisotropic structure of the retina with PS-OCT, whereby the damaged retinal nerve fiber layer (resulting from glaucoma, age-related macular degeneration, or diabetic retinopathy) can be quantified in terms of lateral and depth-dependent abnormal birefringence.¹¹⁻¹³

An emerging direction, in recent years, is the use of polarized light as a standalone modality for characterizing the structural properties of bulk biological tissues.¹⁴⁻³⁸ Such bulk tissue polarimetry is challenging, since the heterogenous and highly scattering nature of biological tissues causes extensive light depolarization and, thus, loss of polarization signal information. Short of getting rid of this problem altogether (as done in microscopy, through the use of thin slices) or partially negating it through depth gating (superficial layer imaging via OCT or confocal approaches), examining bulk tissues has to be done in the presence of severe light diffusion and, thus, polarization signal loss. Fortunately, sensitive measurement and data analysis methods have been developed recently to address this depolarization challenge. Most bulk tissue polarimetric methods can now yield well-resolved lateral images, but offer cumulative polarization properties through the interrogated depth direction. However, bulk tissue polarimetric methods have the advantage of being less complex, less expensive, sensitive to larger sampling depths, and easier and faster to implement

*Address all correspondence to: Alex Vitkin, E-mail: Alex.Vitkin@mp.uhn.on.ca

for a large lateral field of view than the depth-resolved imaging modalities.

As explained in greater detail in the next section, many emerging approaches are based on measuring the bulk tissue's complete polarimetric transfer function, known as its Mueller matrix. This is an information-rich tissue signature that contains the full polarization information reflecting its biophysical properties. However, its measurement, while important and often challenging, is only the first step, and given the abundance of information this matrix contains, further analysis must be used to isolate out the separate distinct biophysical polarization metrics. The Mueller matrix, thus, analyzed via various decomposition methods can then yield various optical effects, including the tissue's linear retardance (proportional to linear birefringence/tissue anisotropy), circular retardance (proportional to circular birefringence/chiral molecule content), and depolarization.^{17–22} Depolarization abnormalities, arising from changes in tissue scattering and absorption properties (transport albedo), are related to alterations in the stroma (e.g., collagen remodeling) and cellular compartment disorders (e.g., nuclear enlargement).^{23–27} Given the fundamental and clinical importance of these and related changes, Mueller matrix polarimetry yielding depolarization and retardance has been used in a variety of (mostly preclinical) studies. A partial list includes differentiating different tissue types, identifying skin cancer lesions, detecting oral precancerous tissue in animal models, visualizing cervical cancer margins in excised samples, locating myocardial infarctions and observing their regeneration following stem-cell therapy, finding the relation between the distension pressure and anisotropy in bladder wall, identifying bladder obstruction disorders, and imaging collagen structure in *ex vivo* tissue of animal models.^{28–36}

As evidenced by such variety, bulk tissue polarimetry holds much promise in biomedicine, but as with any new methodology, many significant challenges remain. In this paper, we summarize the status of the polarimetric field, outline possible emerging improvements, and speculate on its future deployment in biomedicine. We begin with an introduction to the Mueller

matrix methodology, follow with a brief synopsis of recent developments in the instrumentation, and discuss the remaining challenges in the translation of polarimetry into a standalone diagnostic tool. Illustrative application examples and potential future directions of tissue polarimetry are provided throughout.

2 Mueller Matrix Polarimetry in Bulk Tissues: Methodologies and Illustrative Examples

The simplest polarimetric method to examine the properties of a turbid medium, such as tissue, is to illuminate it with a known polarization state (mathematically described by the four-elements incident Stokes vector S_{in}) and to detect the change in polarization of the light after the interaction (represented by the four-elements output Stokes vector S_{out}) [see Fig. 1(a)]. Stokes vectors can describe fully or partially polarized optical beams and, thus, are well suited for describing polarized light-tissue interactions. Comparing the polarization of the incident and the collected light after interaction with the sample can then yield some metrics (e.g., light depolarization) associated with various tissue properties. For instance, Backman et al. developed a theoretical model of polarized light propagation in cells and experimentally showed that the spectrum of polarized light backscattered from the epithelial layers has a distinct fingerprint, which depends on the size of the cells and nuclei, and their refractive indices.²⁵ Recently, Ghassemi et al. showed that different roughness in melanoma lesions leads to abnormal polarization changes and loss of the degree of light polarization. They used this criterion for *in vivo* differentiation of melanoma, benign nevi, and normal skin.³⁷ Analogously, Kunnen et al. recently mapped the measured S_{out} onto the surface of the Poincare sphere, which visualizes the Stokes vector in a three-dimensional (3-D) space with the axes being pure states corresponding to each of the three elements, to distinguish tumor from normal lung regions in *ex vivo* tissue samples [Fig. 1(b)].³⁸ These methods work well when comparing different tissue types or normal/abnormal tissues with the same thickness, and in the same detection geometry. In other words, the

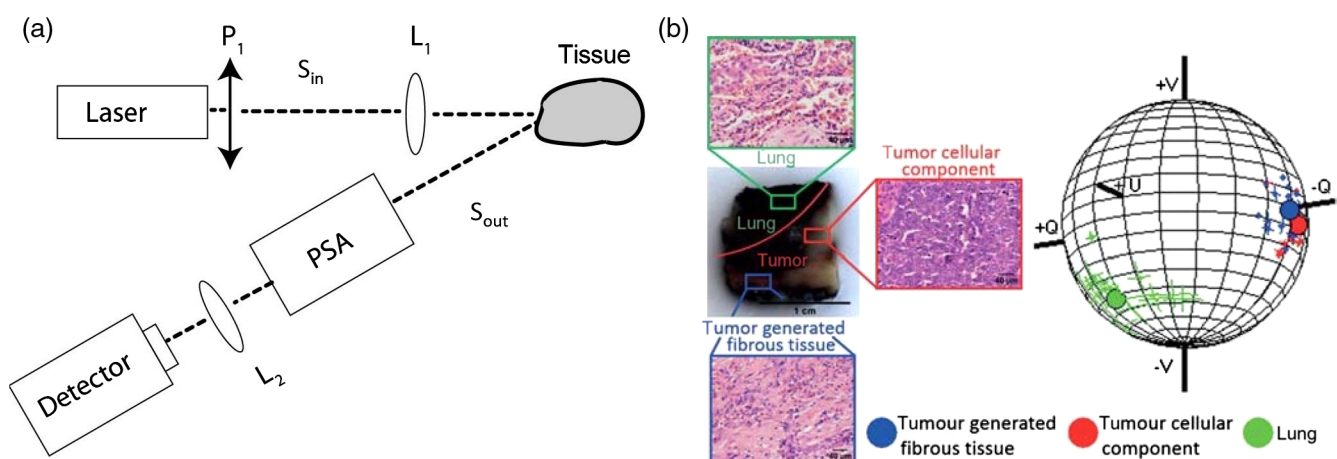


Fig. 1 (a) A Stokes polarimetry point-measurement system, which illuminates the sample with known polarization S_{in} and uses a polarization state analyzer (PSA) to detect the polarization of light after interaction with the sample S_{out} . (b) Experimental results from Ref. 37. Polarization of light after interaction with healthy, premalignant, and tumor regions of *ex vivo* lung tissue are mapped onto the surface of the Poincare sphere. The illumination was circularly polarized in all cases. Each of the three axes Q, U, and V show the pure polarization states linear horizontal or vertical, linear oriented at 45 or -45 deg, and the right or left circular. P_1 is general elliptical polarizer that generates a static elliptical polarization, and L_1 and L_2 are lenses. Figures are produced with permission.

experimental and sample parameters must be tightly controlled for meaningful results comparison and interpretation; this is because the readings are affected by both tissue parameters (quantities of interest) and experimental parameters (e.g., illumination polarization and geometry).

To characterize the polarimetric properties of bulk tissue without admixing uninteresting experimental parameters (e.g., illumination), and without any prior information (i.e., arbitrary and completely unknown turbid media, such as tissue), the full Mueller matrix M should be measured. Mathematically, Mueller matrix M is the medium's polarization transfer function, a 4 by 4 element matrix related to the input and output light polarization by $S_{out} = M \cdot S_{in}$. The Mueller matrices of optical elements, such as polarizers or retarders, can be theoretically calculated from the way they change the polarization of light. But the Mueller matrix of turbid inhomogeneous media, such as tissues, is unpredictable analytically because of the uncertainty in refractive index, size, and location (and nature!) of the scatterers that randomize the photons' propagation paths and result in depolarization. In the special case of well-controlled scattering media (e.g., a turbid phantom composed of uniform-sized microspheres suspended in water), the elements of M may be calculated or approximated, for instance, certain elements set to zero and others set equal (or equal in value and opposite in sign). However, simplifying assumptions are usually not justified in biological tissues, and their measured Mueller matrix elements are generally independent of each other and can have any numerical value from -1 to 1 for a normalized matrix.

For all its advantages, the Mueller matrix is a lumped polarization transfer function of tissue and contains all the simultaneous optical effects, such as scattering, absorption, retardance, and optical activity occurring in the turbid media. The Mueller matrix elements on their own cannot provide detailed information about a sample of tissue with unknown properties. There are, however, several decomposition methods

that help separate these convoluted intermixed effects from the Mueller matrix (more details below) and derive tissues' structural and compositional properties. In recent years, a variety of Mueller matrix decomposition methods have been proposed.^{16,39-42} The very first approach that was successfully applied to bulk biological tissues was Lu-Chipman polar decomposition.¹⁶ As the flow chart in Fig. 2 shows, in this decomposition, the turbid media is modeled as a sequence of a depolarizer, a retarder, and a diattenuator. This is not to say that tissue is intrinsically composed of such elements in such a sequence; rather, this is simply a mathematical representation of polarimetric equivalence, which enables relevant tissue properties to be extracted. Specifically, (1) from the depolarizer matrix, linear, circular, and total depolarization can be calculated. The total depolarization Δ parameter varies with transport albedo and depends on the tissue type.²³⁻²⁷ Next, (2) the retardance matrix can be further decomposed to a linear retardance and a circular retardance matrices;¹⁶ the latter is related to the presence/concentration of biologically interesting chiral substances, such as glucose.^{16,20} From the linear retardance matrix, the tissue strength of the structural anisotropy and its orientation can be retrieved in terms of the optical phase retardance δ (proportional to birefringence) and the fast axis θ ;²⁷⁻³⁶ this is the aspect that is further pursued in this article in greater detail. Finally, (3) diattenuation is another polarization property of limited relevance/importance in biological tissues. Essentially then, Mueller matrix decomposition enables the separation of the depolarization effects resulting from multiple scattering and heterogeneities from other polarization properties, such as the retardance due to structural or compositional anisotropy.

Many groups have used Lu-Chipman polar decomposition of the Mueller matrix for developing diagnostic metrics based on the structural properties. Figure 3 shows representative biomedical applications of Mueller matrix polar decomposition.²⁸⁻³⁶ As will be described in the next section, Mueller matrices were

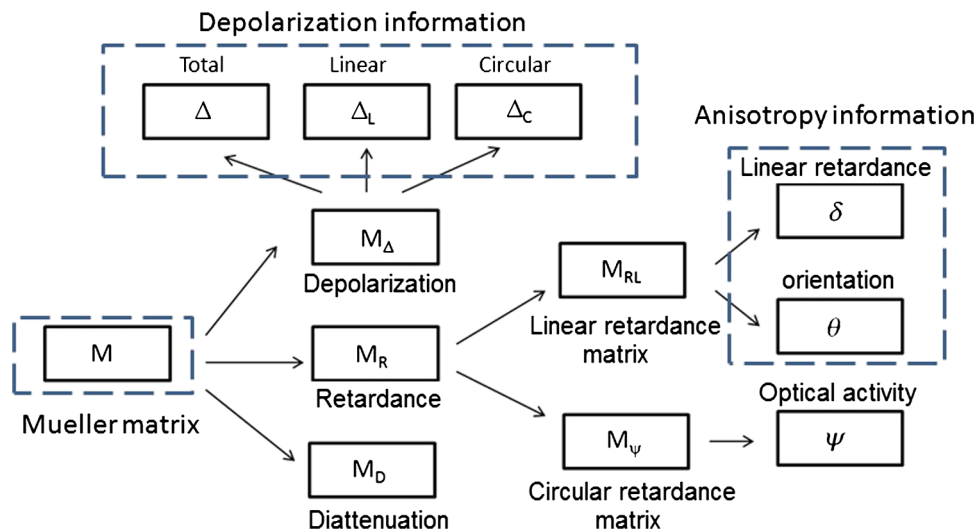


Fig. 2 A flow chart showing the extended version of the Lu-Chipman polar decomposition and its outcome parameters. The tissue Mueller matrix M is first decomposed to a product of a depolarization matrix M_{Δ} , a retardance matrix M_R , and a diattenuation matrix M_D . From M_{Δ} , three parameters, total depolarization Δ , linear depolarization Δ_L , and circular depolarization Δ_C , can be obtained. The matrix M_R can be further decomposed to a product of a linear retardance matrix M_{LR} and circular retardance matrix M_{ψ} . From M_{LR} , the linear retardance δ and the dominant fast axis of anisotropy θ can be derived. From M_{ψ} , the concentration of the chiral molecules ψ can be calculated. M_D is the diattenuation matrix, which is of little relevance to the tissue.

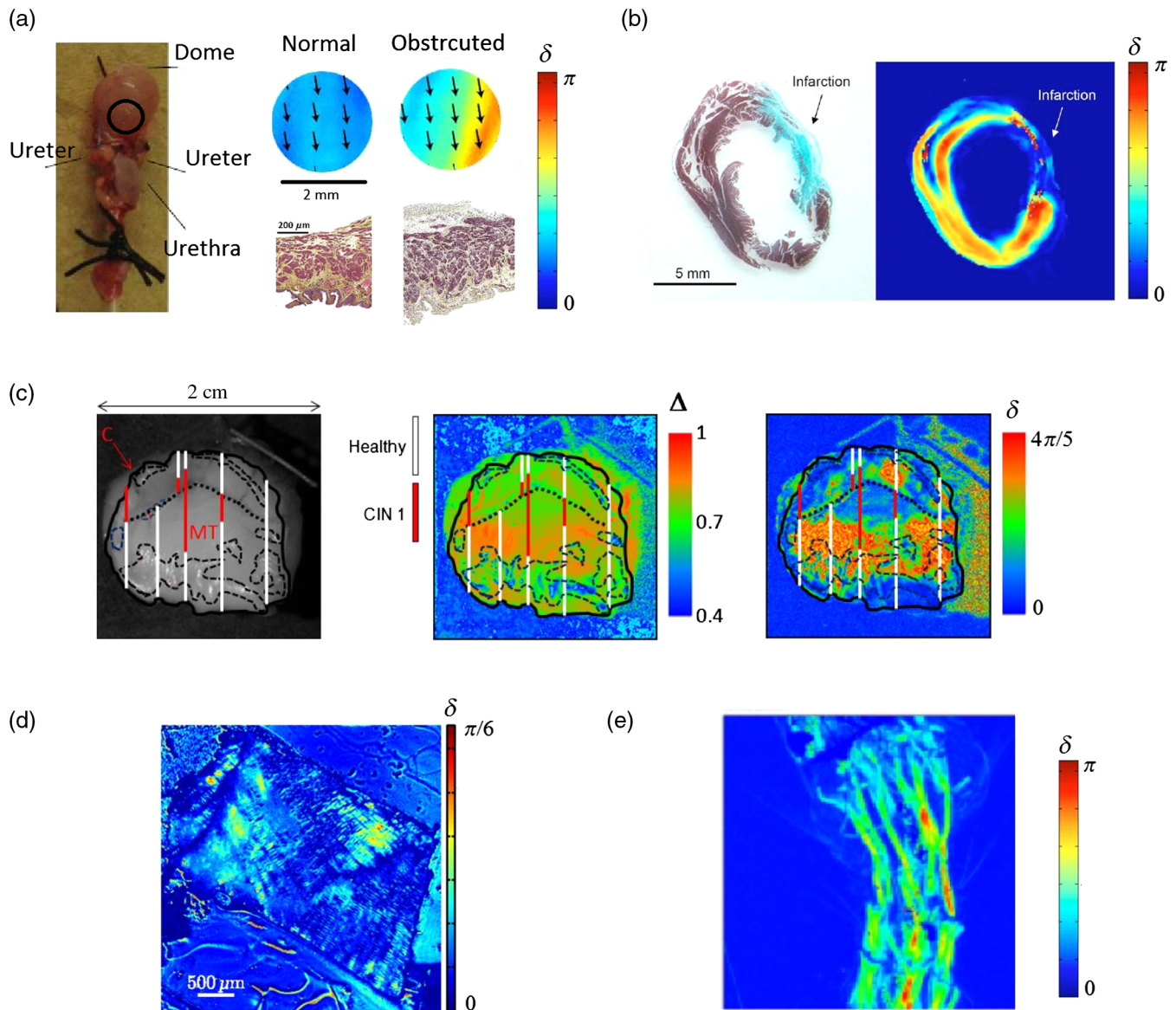


Fig. 3 Examples of biomedical studies showing the applications of Mueller matrix Lu-Chipman polar decomposition. (a) A picture of an *ex vivo* rat bladder; the black circle indicates the ventral region close to the urethra; retardance images (top row) from the ventral region on a normal and obstructed bladder; the arrows show the orientation of the fast axis; their corresponding histology (bottom row), stained with Movat stain. The Mueller matrix was imaged in reflection geometry, by mechanically moving polarizing components.³⁵ (b) Retardance image of an *ex vivo* 1-mm-thick rat myocardium muscle and its respective histology slice. MT indicates malpighian tissue, C shows stroma, and CIN stands for cervical intraepithelial neoplasia. The pink and the blue color in the histology indicate the muscle and the collagen fibers, respectively. The Mueller matrix was imaged in transmission geometry, by mechanically moving polarizing components.³² (c) Photo, total depolarization, and retardance images from a patient *ex vivo* excised cervical tissue. The white lines show regions that were confirmed to be healthy and the red line shows the region that was reported cancerous by histology. The Mueller matrix was imaged in reflection geometry, by a liquid crystal (LC)-based system.³³ (d) Retardance image of a 0.05-mm-thick fresh chicken tendon showing collagen fibers and their organization. The Mueller matrix was imaged in transmission mode by an LC-based system.³⁶ (e) Retardance image of a fly larva (5 \times zoom). The Mueller matrix was measured in transmission geometry by a photoelastic modulator (PEM) based system, Exicor Microlmager (Hinds Instruments⁴³). Figures are produced with permission.

measured with different methods. Figure 3(a) shows an *ex vivo* distended rat bladder and the retardance images taken from the ventral side of the bladder marked with the black circle on the photo. As illustrated, the obstructed bladder shows high retardance compared with the normal bladder. This high retardance as suggested by the corresponding histology may be due to muscle

hypertrophy or extracellular matrix reorganization/deposition.³⁵ Locating these structural disorders is essential for optimal augmentation surgeries and monitoring the tissue functionality following with tissue engineering therapies. Polarized light imaging is the first method to localize these microstructural disorders induced by bladder outlet obstruction while the bladder is

distended and intact; thus, it may have the potential of becoming an imaging modality in urology. Figure 3(b) depicts an *ex vivo* demonstration of using Mueller matrix imaging and its polar decomposition, in detecting the myocardium muscle infarctions in a rat model. As shown, the loss of retardance (anisotropy) in the retardance image is well correlated with deposition of collagen, indicated by the blue color in histology, in place of muscle.³² This indicates the efficacy of polarized light as a research monitoring tool for evaluating the stem-cell therapy treatments for heart infarction, which is the number one cause of heart attacks. Figure 3(c) demonstrates a picture of an *ex vivo* excised tissue of a patient with cervical cancer, and the retardance and the depolarization obtained from decomposing its Mueller matrix. The cancerous regions, indicated by the red lines as opposed to the healthy regions indicated by white, are associated with a loss of retardance and microstructural organization.³³ This suggests that polarized light imaging can be used as a rapid and accurate technique for detecting cancer margins during surgery, thus becoming a standard intraoperative imaging tool. Figures 3(d) and 3(e), respectively, show that the retardance images obtained from polar decomposition can be used for visualizing the well-organized collagen fibers (associated with high retardance) of 50- μm -thick chicken tendon and the different structure in a fly larva.^{36,43} These two examples illustrate the capability of polarized light imaging/polar decomposition for wide-field microscopy and imaging detailed microstructures. From these examples, it is clear that polarized light imaging and polar decomposition of the Mueller matrix are powerful methods for characterizing various tissue microstructures, for various biomedical diagnostic/monitoring applications.

Bulk tissue polarimetry does not, in general, offer depth resolution/discrimination, so the two-dimensional depolarization and retardance images contain accumulated 3-D information over the interrogated depth. Similar to diffuse optical tomography, the optical voxel size of polarized light imaging is a function of light wavelength, measurement geometry, and tissue's optical properties (scattering and absorption). Simulation results from polarization-sensitive Monte Carlo code (Pol-MC) suggest that average pathlength of the polarization preserving photons is ~ 6 mm (in the visible wavelength range and for typical tissue properties).⁴⁴⁻⁴⁶ The interrogation depth then depends on the imaging geometry and the incident polarization state (circular, linear), and can be up to a few millimeters in transmission (~ 4 mm) or in backscattering (~ 2 mm).⁴⁴⁻⁴⁶ The lateral resolution (FWHM of point spread function of the polarization preserving photons in tissue for an incident pencil beam) is ~ 200 μm .⁴⁴ These numbers need further experimental validation with well-controlled phantom studies.

As mentioned before, there are a variety of methods to interpret a bulk tissue's Mueller matrix. Polar decomposition is sequential, meaning that it models tissue as a sequence of a depolarization, retardance, and diattenuation.¹⁶ Perhaps somewhat surprisingly, this assumption works for tissues and model turbid media, as recently validated.²⁸⁻³⁶ However, polar decomposition fails to yield accurate results when the media is made of distinct layers of depolarizer, diattenuator, and retarder in a different sequential order than the polar decomposition sequence. For instance, Ortega-Quijano et al. showed that polar decomposition fails for a medium composed of a polarizer sandwiched between two layers of scattering media.⁴⁷ Another approach, which has received a lot of attention recently, is the differential

decomposition. Here, all the effects, such as depolarization and retardance, are modeled evenly throughout the entire sample and occur simultaneously (versus in sequence as per polar decomposition). In other words, all polarization effects occur simultaneously over infinitesimal propagation distance of light in the tissue. Some studies suggest that differential decomposition may be closer to tissue reality compared with polar decomposition, since it does not operate sequentially.⁴⁷⁻⁴⁹ To test this hypothesis, using Pol-MC code, we recently modeled many bilayered Mueller matrices of heterogeneous birefringent turbid media, with different orientation or value of anisotropy in the layers.⁴⁶ The resultant Mueller matrices were then decomposed with both polar and differential decompositions. Our initial studies (manuscript in preparation) show that these two decompositions yield nearly identical results for a turbid medium that does not contain distinct layers of retarder/diattenuator (as is the case for biological tissues). Thus, it seems that differential decomposition does not offer a great advantage over polar decomposition for biomedical uses.

3 Polarimetric Instrumentation for *Ex Vivo* and *In Vivo* Tissue Diagnosis

Most current polarized light imaging systems that measure the full Mueller matrix of bulk tissues are at the research level. They have been used for *ex vivo* characterization of tissues, intraoperative examination of excised tissues, and initial *in vivo* examinations of retina and skin.^{31-36,50} Regardless of the application, a polarimetric measurement system contains a polarization state analyzer (PSA), which measures the Stokes vector of light after interaction with the sample (see Fig. 4). A complete polarimetric system for measuring the Mueller matrix should also have a polarization state generator (PSG) to control and modulate the polarization of the incident light, as shown in Fig. 4. Biological tissues are highly scattering and heterogeneous; thus, the collected light after interaction with tissue is significantly depolarized. To extract maximum polarimetric information in this challenging low signal-to-noise ratio (SNR) setting, the measurement system should be sensitive (able to sense small changes) and robust (measure the polarization changes reproducibly and accurately).

Several groups have shown that the polarization states generated and read by PSG/PSA can be optimized to yield more accurate and noise-robust recovery of the polarimetric signal.⁵¹⁻⁵⁴ In addition to selecting the polarization states to optimize measurement accuracy, the measurement system should be carefully calibrated. The calibration procedures vary for different systems employing different polarization modulation components. However, in a rigorous study, Compain et al. suggested a general calibration procedure, applicable to any polarimetric system, regardless of the optics and optoelectronic modulation methods.⁵⁵ With the novel advances in polarimetric systems, we believe that this procedure will be widely adopted in the next few years.

There are a variety of polarimetric measurement systems with different SNRs and sensitivities. Point measurement systems with low noise photodetectors and electronic lock-in detection are the most sensitive. For example, these point-sensing systems can be used for sensing small concentrations of glucose by measuring optical activity, or they can be used for detecting tissue microstructure with a point-by-point scanning approach with high sensitivity.^{20,56-58} However, imaging systems are more suitable for examining large areas (regions) of biological

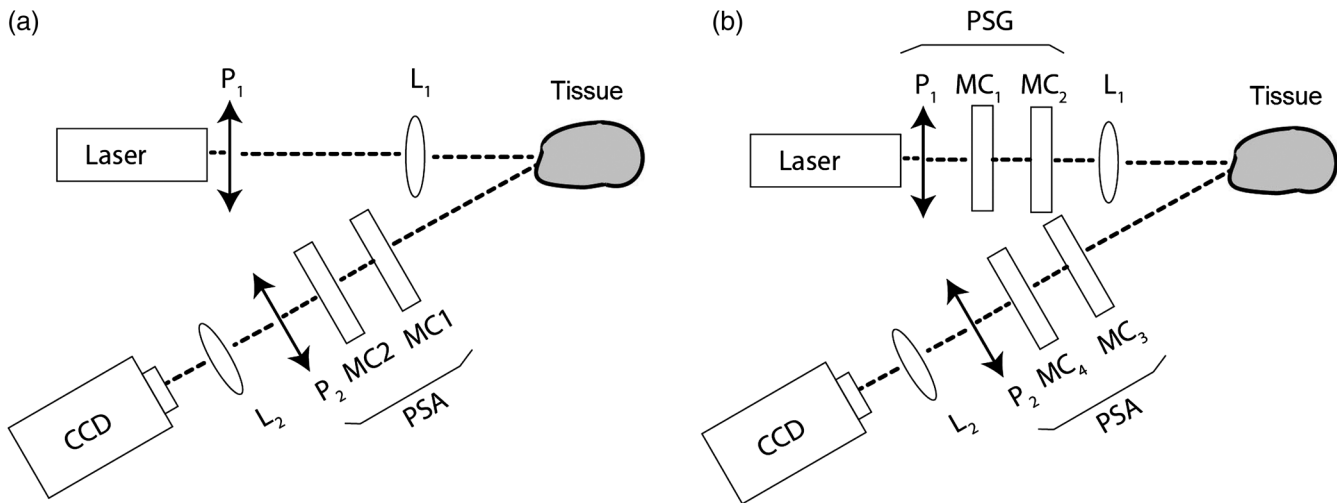


Fig. 4 (a) Stokes polarimetry imaging system [cf the point-measurement system in Fig. 1(a)]. The PSA can be made of two modulating components (MCs), such as two LCs or two PEMs, or two pairs of grating/prisms. (b) Mueller matrix imaging system, which is composed of a polarization state generator (PSG) and a PSA, each having two MCs that generate/analyze several polarization states. P_1 and P_2 are polarizing components that can generate or select a static elliptical polarization state, and L_1 and L_2 are lenses.

tissues, which often show variations in the lateral direction. An ideal tissue polarimetry imaging system should be fast, robust, accurate, and provide high resolution over a large field of view. These characteristics depend on the modulating components in the PSG/PSA. Polarization can be modulated electronically by liquid crystals (LCs) or photoelastic modulators (PEMs), mechanically by rotating linear polarizers and quarter waveplates, and by diffraction using polarizing prisms, gratings, or graded index lenses.^{59–72} In recent years, the field has witnessed many advanced designs and approaches, and there have been several demonstrations of using these novel systems for imaging biological tissues (Fig. 3). Systems devoid of any mechanically moving parts are certainly preferred. LC- and PEM-based systems are both capable of imaging in millisecond time scales. LCs are easier to switch electronically and can be used for arbitrary set of polarization states that result in improved measurement accuracy of the Mueller matrix.⁶⁰ PEMs can only modulate the retardance in a sinusoidal fashion; however, they have larger clear aperture well suited for imaging over a large field of view.^{67,69} Snapshot systems, based on diffractive components, are the fastest, but they use spatial frequency filters, which reduce the amount of imaging information and may be suboptimal for high-resolution imaging over a large field of view.⁷⁰

One emerging direction in polarized light imaging is combining the measurement instruments with wide-field depth-resolved techniques. For example, a very plausible direction might be its combination with modulated imaging. Modulated imaging is a diffuse reflectance imaging modality to measure the optical properties of the tissue with limited depth-resolved capability in a relatively short time.⁷³ Optical properties are beneficial for tissue differentiation and correction of fluorescence signals in image guided surgery. Since modulated imaging and Mueller matrix imaging both aim to characterize bulk tissues, one can combine them to potentially increase signal information content, specially for potential intraoperative biomedical diagnostics.

Finally, as mentioned, polarized light has been shown to effectively detect *ex vivo* tissue disorders of internal organs, such as the heart, cervix, and bladder.^{32–35} Reaching these organs deep within the body can enable *in vivo* deployment;

therefore, polarimetric optical delivery/pick-up methods not based on free-space optics must be developed. These include various varieties of rigid or flexible waveguides, fibers, and catheters. This is challenging in that these optical delivery vehicles often distort the polarization states of the light they transmit; this will produce large signal artifacts that will likely overwhelm the weak tissue polarization signals these delivery vehicles are meant to relay. One promising solution to avoid this problem is the use of distal polarization components, which has been suggested by several researchers.^{74,75} Using distal polarizers facilitates accurate generation of polarized illumination and collection of the polarized light backscattered from the tissue. Using this concept, our group is in the process of fabricating a fiber optic probe with distal polarizing components for measuring the full tissue Mueller matrix (manuscript in preparation). This approach of using distal polarizing components has also been used in wide-field endoscopes; for instance, as shown in Figs. 5(a) and 5(b), Qi et al. incorporated moving polarizers at the proximal and distal ends of a commercially available laparoscope (1 cm outer diameter, rigid construction) to measure the linear part of the Mueller matrix.⁷⁶ The first row and first column of the 4×4 Mueller matrix are, thus, not measured, often due to difficulties in generating and transmitting circularly polarized light. As illustrated in Figs. 5(c)–5(e), this modified laparoscope was used to measure the depolarization and the retardance of different organs in an open rat abdomen *in vivo*.⁷⁶ As expected, the organs have different scattering, absorption, and morphological characteristics and, thus, can be differentiated with specific ranges of retardances and depolarizations. Another alternative is to use polarization maintaining fibers for delivery/collection of light and a PSA and a PSG at the proximal ends to modulate the polarization. For example, in a very recent report, Vizet et al. demonstrated full 4×4 Mueller matrix measurements through a single polarization maintaining fiber. To correct for random changes in the fiber optical axis, which changes the polarization at the sample compared with the proximal end, a switchable calibration mirror was used.⁷⁷ This is similar to the calibration procedure applied in some PS-OCT systems that corrects the axis with the signal

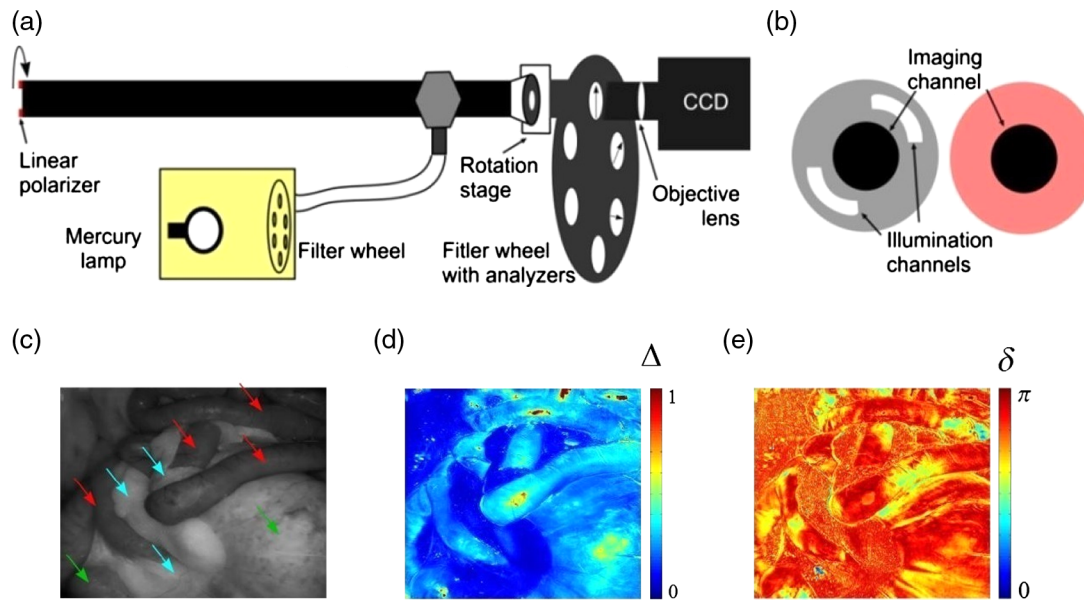


Fig. 5 (a) The modified commercial endoscope for imaging the linear part of the Mueller matrix. At the proximal end and before the camera, a wheel of different polarizers is used to select different polarizations of the backscattered light from the tissue. (b) The unmodified distal end of the endoscope, shown by gray, is covered with a ring-shaped linear polarizer sheet shown in pink. The endoscope rotates from the proximal end to change the orientation of the linear polarizer sheet at the distal end and illuminates the tissue with different polarizations (after Qi et al.⁷⁶). (c) Photograph of a rat abdomen. The red arrows indicate the small bowel, white arrows show the large intestine, and the yellow mark the fat (after Qi et al.⁷⁶). (d) Total depolarization image of the area shown in (c). The linear part of the Mueller matrix was measured with the modified endoscope at the wavelength of 546 nm, and the depolarization was obtained from Mueller matrix polar decomposition. (e) Corresponding retardance image of the area shown in (c). The linear part of the Mueller matrix was measured by the modified endoscope at wavelength of 546 nm, and the retardance was obtained from the Mueller matrix decomposition. Figures are produced with permission.⁷⁶

reflected back from the tissue surface. The details are not described in peer-reviewed publications yet, but are likely forthcoming. These developments will eventually enable *in vivo* polarimetry of deep-seated tissue pathologies in the near future, most likely in the cystoscopy/endoscopy/bronchoscopy settings.

4 Summary

United Nations has designated 2015 as the International Year of Light, and it is entirely fitting that a tissue assessment approach based on polarized light becomes an important player in diagnostic photomedicine in this time frame. After all, polarimetry has had a long and distinguished history in science, industry, and medicine,⁷⁸ albeit primarily in transparent media and thin films; it is now poised to make its mark in examining thick biological tissues. The ability to retrieve structural properties of bulk tissues opens up many possibilities in biomedical applications, including fast intraoperative/laparoscopic diagnosis and simple low-cost cystoscopic/endoscopic screening. The most recent advances in the field are based on measuring (and decomposing) the tissue Mueller matrix, which contains all the relevant tissue biophysical properties accessible by polarimetry. The most promising directions in polarimetric imaging, including applications, analyses, and instrumentation as outlined in this paper, demonstrate the resurgent interest and rapid progress in the field. Despite these recent advances, translating polarimetry *in vivo* and eventually into the clinic remains a challenge. Further advances that may facilitate this are development of more accurate Mueller matrix interpretation methods,

improvements in measurement techniques and instrumentation (including optical delivery and pick-up probes that do not distort polarization upon transmission), combination with other wide-field imaging modalities, and applications to specific biomedical diagnostic problems.

References

1. J. Tewari, R. Mehrotra, and J. Irudayaraj, "Direct near infrared analysis of sugar cane clear juice using a fibre-optic transmittance probe," *J. Near Infrared Spectrosc.* **11**(1), 351–356 (2003).
2. P. B. Russell et al., "A multiparameter aerosol classification method and its application to retrievals from spaceborne polarimetry," *J. Geophys. Res. Atmos.* **119**(16), 9838–9863 (2014).
3. M. Losurdo et al., "Spectroscopic ellipsometry and polarimetry for materials and systems analysis at the nanometer scale: state-of-the-art, potential, and perspectives," *J. Nanopart. Res.* **11**(7), 1521–1554 (2009).
4. R. D. Allen, J. Brault, and R. D. Moore, "A new method of polarization microscopic analysis," *J. Cell Biol.* **18**, 223–235 (1963).
5. D. Axelrod, "Carbocyanine dye orientation in red cell membrane studied by microscopic fluorescence polarization," *Biophys. J.* **26**(3), 557–573 (1979).
6. A. M. Vrabioiu and T. J. Mitchison, "Structural insights into yeast septin organization from polarized fluorescence microscopy," *Nature* **443**, 466–469 (2006).
7. F. Vasefi et al., "Polarization-sensitive hyperspectral imaging *in vivo*: a multimode dermoscope for skin analysis," *Sci. Rep.* **4**, 4924 (2014).
8. J. F. de Boer et al., "Two-dimensional birefringence imaging in biological tissue by polarization-sensitive optical coherence tomography," *Opt. Lett.* **22**(12), 934–936 (1997).

9. S. Jiao and L. V. Wang, "Two-dimensional depth-resolved Mueller matrix of biological tissue measured with double-beam polarization-sensitive optical coherence tomography," *Opt. Lett.* **27**(2), 101–103 (2002).
10. P. J. Campagnola and L. M. Loew, "Second-harmonic imaging microscopy for visualizing biomolecular arrays in cells, tissues and organisms," *Nat. Biotechnol.* **21**, 1356–1360 (2003).
11. M. Pircher, C. K. Hitzenberger, and U. Schmidt-Erfurth, "Polarization sensitive optical coherence tomography in the human eye," *Prog. Retin. Eye Res.* **30**(6), 431–451 (2011).
12. B. Cense et al., "In vivo birefringence and thickness measurements of the human retinal nerve fiber layer using polarization-sensitive optical coherence tomography," *J. Biomed. Opt.* **9**(1), 121–125 (2004).
13. X. Huang and R. W. Knighton, "Microtubules contribute to the birefringence of the retinal nerve fiber layer," *Invest. Ophthalmol. Vis. Sci.* **46**(12), 4588–4593 (2005).
14. S. G. Demos and R. R. Alfano, "Optical polarization imaging," *Appl. Opt.* **36**, 150–155 (1997).
15. S. L. Jacques, J. C. R. Ramella, and K. Lee, "Imaging skin pathology with polarized light," *J. Biomed. Opt.* **7**, 329–340 (2002).
16. S. Lu and R. A. Chipman, "Interpretation of Mueller matrices based on polar decomposition," *J. Opt. Soc. Am. A* **13**, 1106–1113 (1996).
17. J. J. Gil and E. Bernabeu, "Obtainment of polarizing and retardation parameters of a non-depolarizing optical system from the polar decomposition of its Mueller matrix," *Optik* **76**(2), 67–71 (1987).
18. S. Manhas et al., "Mueller matrix approach for determination of optical rotation in chiral turbid media in backscattering geometry," *Opt. Express* **14**(1), 190–202 (2006).
19. N. Ghosh, M. F. G. Wood, and I. A. Vitkin, "Influence of the order of the constituent basis matrices on the Mueller matrix decomposition-derived polarization parameters in complex turbid media such as biological tissues," *Opt. Commun.* **283**, 1200–1208 (2010).
20. M. F. G. Wood, N. Ghosh, and I. A. Vitkin, "Mueller matrix decomposition for extraction of individual polarization parameters from complex turbid media exhibiting multiple scattering, optical activity, and linear birefringence," *J. Biomed. Opt.* **13**, 044036 (2008).
21. M. F. G. Wood et al., "Proof-of-principle demonstration of a Mueller matrix decomposition method for polarized light tissue characterization in vivo," *J. Biomed. Opt.* **14**, 014029 (2009).
22. M. A. Wallenburg et al., "Polarimetry-based method to extract geometry-independent metrics of tissue anisotropy," *Opt. Lett.* **35**, 2570 (2010).
23. V. Sankaran, J. T. Walsh, and D. J. Maitland, "Comparative study of polarized light propagation in biological tissues," *J. Biomed. Opt.* **7**, 300–306 (2002).
24. S. Alali et al., "Quantitative correlation between light depolarization and transport albedo of various porcine tissues," *J. Biomed. Opt.* **17**(4), 045004 (2012).
25. V. Backman et al., "Polarized light scattering spectroscopy for quantitative measurement of epithelial cellular structures in situ," *IEEE J. Sel. Topics Quantum Electron.* **5**(4), 1019–1026 (1999).
26. M. Barlett et al., "Measurement of particle size distribution in mailman cells in vitro by use of polarized light spectroscopy," *Appl. Opt.* **43**, 1296–1307 (2004).
27. M. Schmitt, A. H. Gandjbakhche, and R. F. Bonner, "Use of polarized light to discriminate short-path photons in a multiply scattering medium," *Appl. Opt.* **31**, 6535–6546 (1992).
28. M. H. Smith et al., "Mueller matrix imaging polarimetry in dermatology," *Proc. SPIE* **3911**, 1605–7422 (2000).
29. J. Chung et al., "Use of polar decomposition for the diagnosis of oral precancer," *Appl. Opt.* **46**(15), 3038–3045 (2007).
30. X. Li and G. Yao, "Mueller matrix decomposition of diffuse reflectance imaging in skeletal muscle," *Appl. Opt.* **48**(14), 2625–2631 (2009).
31. G. L. Liu, Y. Li, and B. D. Cameron, "Polarization-based optical imaging and processing techniques with application to the cancer diagnostics," *Proc. SPIE* **4617**, 208–220 (2002).
32. M. F. G. Wood et al., "Polarization birefringence measurements for characterizing the myocardium, including healthy, infarcted, and stem-cell-regenerated tissues," *J. Biomed. Opt.* **15**, 047009 (2010).
33. A. Pierangelo et al., "Polarimetric imaging of uterine cervix: a case study," *Opt. Express* **21**(12), 14120–14130 (2013).
34. S. Alali et al., "Optical assessment of tissue anisotropy on ex vivo distended rat bladders," *J. Biomed. Opt.* **17**(8), 086010 (2012).
35. S. Alali et al., "Assessment of local structural disorder of the bladder wall in partial bladder outlet obstruction using polarized light imaging," *Biomed. Opt. Express* **5**(2), 621–629 (2014).
36. P. G. Ellingsen et al., "Mueller matrix three dimensional imaging of collagen fibers," *J. Biomed. Opt.* **19**(2), 026002 (2014).
37. P. Ghassemi et al., "Out-of-plane Stokes imaging polarimeter for early skin cancer diagnosis," *J. Biomed. Opt.* **17**(7), 076014 (2012).
38. B. Kunnen et al., "Application of circularly polarized light for non-invasive diagnosis of cancerous tissues and turbid tissue-like scattering media," *J. Biophotonics*, 1–7 (2014).
39. J. J. Gil, I. San José, and R. Ossikovski, "Serial-parallel decompositions of Mueller matrices," *J. Opt. Soc. Am. A* **30**(1), 32–50 (2013).
40. R. Ossikovski, "Differential matrix formalism for depolarizing anisotropic media," *Opt. Lett.* **36**, 2330–2332 (2011).
41. N. Ortega-Quijano and J. L. Arce-Diego, "Mueller matrix differential decomposition," *Opt. Lett.* **36**, 1942–1944 (2011).
42. L. Martin et al., "Analysis of experimental depolarizing Mueller matrices through a hybrid decomposition," *Appl. Opt.* **54**(1), 27–36 (2014).
43. <http://www.hindsinstruments.com/products/exicor-micro-imager/> (October 2015).
44. X. Guo, M. F. G. Wood, and I. A. Vitkin, "A Monte Carlo study of penetration depth and sampling volume of polarized light in turbid media," *Opt. Commun.* **281**, 380–387 (2008).
45. X. Guo, M. F. G. Wood, and A. Vitkin, "Monte Carlo study of path-length distribution of polarized light in turbid media," *Opt. Express* **15**(3), 1348–1360 (2007).
46. S. Alali, Y. Wang, and I. A. Vitkin, "Detecting axial heterogeneity of birefringence in layered turbid media using polarized light imaging," *Biomed. Opt. Express* **3**(12), 3250–3263 (2012).
47. N. Ortega-Quijano et al., "Experimental validation of Mueller matrix differential decomposition," *Opt. Express* **20**(2), 1151–1163 (2012).
48. S. Kumar et al., "Comparative study of differential matrix and extended polar decomposition formalisms for polarimetric characterization of complex tissue-like turbid media," *J. Biomed. Opt.* **17**(10), 105006 (2012).
49. M. Villiger and B. E. Bouma, "Practical decomposition for physically admissible differential Mueller matrices," *Opt. Lett.* **39**(7), 1779–1782 (2014).
50. K. M. Twietmeyer et al., "Mueller matrix retinal imager with optimized polarization conditions," *Opt. Express* **16**(26), 21339–21354 (2008).
51. A. Ambirajan and J. D. C. Look, "Optimum angles for a polarimeter: part I," *Opt. Eng.* **34**(6), 1651–1655 (1995).
52. J. S. Tyo, "Design of optimal polarimeters: maximization of signal-to-noise ratio and minimization of systematic error," *Appl. Opt.* **41**(4), 619–630 (2002).
53. K. M. Twietmeyer and R. A. Chipman, "Optimization of Mueller matrix polarimeters in the presence of error sources," *Opt. Express* **16**(15), 11589–11603 (2008).
54. D. Layden, M. F. G. Wood, and I. A. Vitkin, "Optimum selection of input polarization states in determining the sample Mueller matrix: a dual photoelastic polarimeter approach," *Opt. Express* **20**(18), 20466–20481 (2012).
55. E. Compain, S. Poirier, and B. Drévilion, "General and self-consistent method for the calibration of polarization modulators, polarimeters, and Mueller-matrix ellipsometers," *Appl. Opt.* **38**(16), 3490–3502 (1999).
56. C. E. F. do Amaral and B. Wolf, "Current development in non-invasive glucose monitoring," *Med. Eng. Phys.* **30**(5), 541–549 (2008).
57. B. D. Cameron et al., "The use of polarized laser light through the eye for noninvasive glucose monitoring," *Diabetes Technol. Ther.* **1**(2), 135–143 (1999).
58. M. F. G. Wood, D. Côté, and I. A. Vitkin, "Combined optical intensity and polarization methodology for analyte concentration determination in simulated optically clear and turbid biological media," *J. Biomed. Opt.* **13**(4), 044037 (2008).
59. J. S. Baba et al., "Development and calibration of an automated Mueller matrix polarization imaging system," *J. Biomed. Opt.* **7**(3), 341–349 (2002).
60. P. A. Letnes et al., "Fast and optimal broad-band Stokes/Mueller polarimeter design by the use of a genetic algorithm," *Opt. Express* **18**(22), 23095–23103 (2010).

61. G. Caurel, A. D. Martino, and B. Drévilion, "Spectroscopic Mueller polarimeter based on liquid crystal devices," *Thin Solid Films* **455–456**, 120–123 (2004).
62. D. J. Diner et al., "First results from a dual photoelastic-modulator-based polarimetric camera," *Appl. Opt.* **49**(15), 2929–2946 (2010).
63. R. C. Thompson, J. R. Bottiger, and E. S. Fry, "Measurement of polarized light interactions via the Mueller matrix," *Appl. Opt.* **19**(8), 1323–1332 (1980).
64. R. C. Thompson, J. R. Bottiger, and E. S. Fry, "Measurement of polarized light interactions via the Mueller matrix," *Appl. Opt.* **19**(8), 1323–1332 (1980).
65. C. Y. Han and Y. F. Chao, "Photoelastic modulated imaging ellipsometry by stroboscopic illumination technique," *Rev. Sci. Instrum.* **77**(2), 023107 (2006).
66. O. Arteaga et al., "Mueller matrix polarimetry with four photoelastic modulators: theory and calibration," *Appl. Opt.* **51**(28), 6805–6817 (2012).
67. S. Nichols et al., "Imaging with photoelastic modulators," *Proc. SPIE* **9099**, 909912 (2014).
68. S. Alali and I. A. Vitkin, "Optimization of rapid Mueller matrix imaging of turbid media using four photoelastic modulators without mechanically moving parts," *Opt. Eng.* **52**(10), 103114 (2013).
69. S. Alali, T. Yang, and I. A. Vitkin, "Rapid time-gated polarimetric Stokes imaging using photoelastic modulators," *Opt. Lett.* **38**(16), 2997–3000 (2013).
70. H. Luo et al., "Compact and miniature snapshot imaging polarimeter," *Appl. Opt.* **47**(24), 4413–4417 (2008).
71. M. W. Kudenov et al., "Snapshot imaging Mueller matrix polarimeter using polarization gratings," *Opt. Lett.* **37**, 1367–1369 (2012).
72. J. Chang et al., "Single-shot spatially modulated Stokes polarimeter based on a GRIN lens," *Opt. Lett.* **39**(9), 2656–2659 (2014).
73. D. J. Cuccia et al., "Modulated imaging: quantitative analysis and tomography of turbid media in the spatial-frequency domain," *Opt. Lett.* **30**(11), 1354–1356 (2005).
74. A. Myakov et al., "Fiber optic probe for polarized reflectance spectroscopy in vivo: design and performance," *J. Biomed. Opt.* **7**(3), 388–397 (2002).
75. V. M. Turzhitsky et al., "Measuring mucosal blood supply in vivo with a polarization gating probe," *Appl. Opt.* **47**(32), 6046–6057 (2008).
76. J. Qi et al., "Polarized multispectral imaging in a rigid endoscope based on elastic light scattering spectroscopy," *Biomed. Opt. Express* **3**(9), 2087–2099 (2012).
77. J. Vizet et al., "Demonstration of Mueller polarimetry through an optical fiber for endoscopic applications," presented at *CLEO: QELS Fundamental Science Poster Session 2 (JW2A)*, 8–13, OSA, San Jose, California (2014).
78. I. A. Vitkin, "Polarized light and the asymmetry of life," *Opt. Photonics News* **7**, 30–33 (1996).

Sanaz Alali is currently a research fellow at Wellman Center for Photomedicine (Harvard Medical School and Massachusetts General Hospital in Boston, United States), where she works on developing *in vivo* microscopy technologies. She has received her PhD degree in medical biophysics (biophotonics) from the University of Toronto in Canada in 2014. Her PhD was focused on polarized light imaging instrumentation and applications for biomedical diagnosis and she has authored several papers in this field.

Alex Vitkin is a professor of medical biophysics and radiation oncology at the University of Toronto, a senior scientist at the Ontario Cancer Institute, and a clinical medical physicist at Princess Margaret Hospital (Toronto, Ontario, Canada). He has published over 140 papers and book chapters on diagnostic and therapeutic uses of light in biomedicine, and currently serves as a topical editor of optics letters. He is also a board-certified medical physicist and a fellow of OSA and SPIE.